The Harvard Sequence and Fraunhofer Line Strength

Håkon Fossheim

Institute of Theoretical Astrophysics, P.O. Box 1029, Blindern, N–0315 Oslo, Norway

Abstract. By following in the footsteps of Cecilia Payne, the hydrogen spectral lines in the Harvard sequence were determined to be the Balmer series. Under the assumption that line strength scales linearly with the lower energy level population density of an atom, the Boltzmann distribution was applied to find that the lower energy levels are more populated than higher energy levels. A comparison between the Ca^+K line and the H_α line was made by using the Boltzmann- and Saha distributions. The calculations confirmed that the Ca^+K line should indeed be stronger for stellar atmospheres similar to the sun. The temperatures at which stellar photospheres with electron pressure $P_e = 10^2$ dyne cm^{-2} have a hydrogen ionization fraction of 50% was determined to be 9260 K.

1. Introduction

To understand the formation of spectral lines, the Boltzmann- and Saha distributions are key. They describe the population density of a given energy level or a certain ionization stage. When Cecilia Payne wrote her thesis in 1925, she assumed that the strength of spectral lines scale linearly with the population of the lower energy level corresponding to the line. This is roughly true, although the scaling is nonlinear through a "curve of growth" as will be seen.

Payne's theses was on the frontier of spectroscopy and was dubbed "undeoubtedly the most brilliant PhD theses ever written in astronomy" by Otto Struve (1). It is worthy of study even today.

2. Theory and Results

2.1. Linestrength

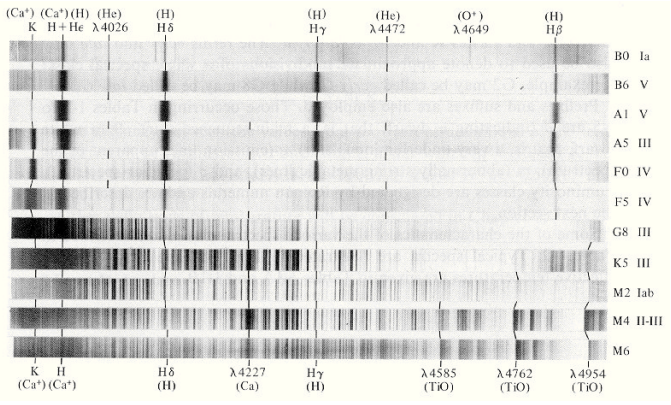

Fig. 1: The Harvard Sequence. The image is positive. Each horizontal stripe correspond to the spectrum of a star, and it's classification is specified in the right column. Wavelengths increase to the right, and are given in Ångstrøm. The image is taken from (1).

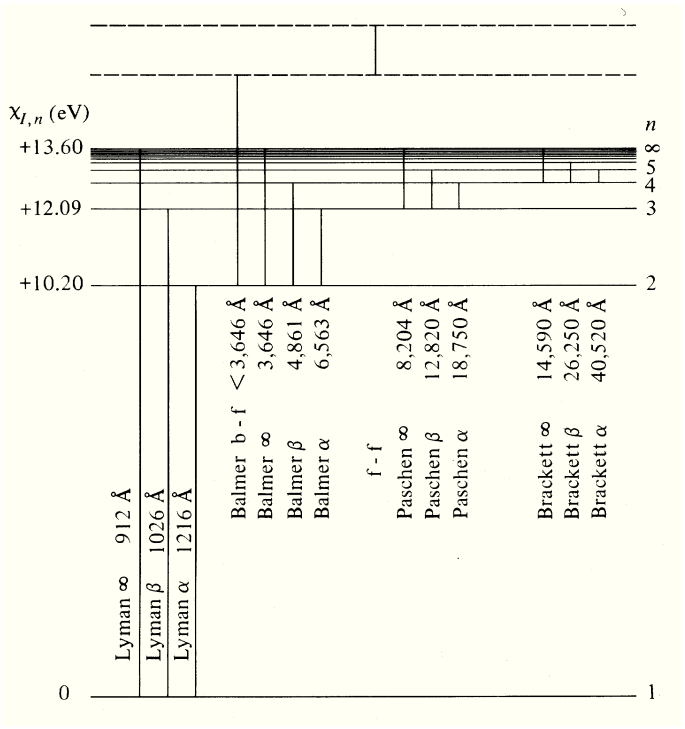

Fig. 2: Excitation energies for the Hydrogen atom. The Lyman, Balmer, Paschen and Bracket series are represented with lines corresponding to the energy level transition the electron has to make to emit/absorb the photon given under the line. Taken from (1).

From figure 1 it can be seen that the H_β line has a wavelength in the range 4762-4954Å. The corresponding transition in figure 2 is from $n = 4$ to $n = 2$, namely the Balmer β line. The rest of the hydrogen lines all have wavelengths larger than the Balmer ∞ line, but smaller than that of the Balmer β line.

- H_β: Balmer β (s=4 → s=2)
- H_γ: Balmer γ (s=5 → s=2)
- H_δ: Balmer δ (s=6 → s=2)
- H_ϵ: Balmer ϵ (s=7 → s=2)

All of these transitions share the lower level, and none share the upper level. Payne's basic assumption was that the strength of the absorption lines scale linearly with the population density of the lower level. In reality the scaling isn't linear. Her reason for assuming this might have been that the higher the population density of the lower level, the more electrons can get excited and de-excited, creating a stronger spectral line.

2.2. The Boltzmann and Saha distributions

From the Boltzmann distribution given by equation 3, a rough estimate of the relative line strengths for the α lines can be given. In this rough estimate, the statistical weight and the partition function are ignored, and the temperature is set to that of the surface of the sun, $T = 5778K$.

$$n_{r,s} \propto e^{-\frac{\chi_{r,s}}{kT}} \propto \text{Line Strength (LS)} \tag{1}$$

$$\frac{\text{LS(Lyman } \alpha)}{\text{LS(Balmer } \alpha)} = \frac{e^{-\frac{\chi_{1,1}}{kT}}}{e^{-\frac{\chi_{1,2}}{kT}}} \approx 7.88 \cdot 10^8$$

$$\frac{\text{LS(Balmer } \alpha)}{\text{LS(Paschen } \alpha)} = \frac{e^{-\frac{\chi_{1,2}}{kT}}}{e^{-\frac{\chi_{1,3}}{kT}}} \approx 44.5$$

$$\frac{\text{LS(Paschen } \alpha)}{\text{LS(Bracket } \alpha)} = \frac{e^{-\frac{\chi_{1,3}}{kT}}}{e^{-\frac{\chi_{1,4}}{kT}}} \approx 3.76$$

$\chi_{1,1}, \chi_{1,2}$ and $\chi_{1,3}$ are shown explicitly in figure 2, whilst $\chi_{1,4}$ was found using

$$\chi_{1,4} - \chi_{1,3} = \frac{hc}{\lambda} \tag{2}$$

and inserting for the wavelength of the Paschen α line.

In thermodynamic equilibrium (TE) the partitioning of a specific atom or ion stage over its given discrete energy levels is given by the Boltzmann distribution:

$$\frac{n_{r,s}}{N_r} = \frac{g_{r,s}}{U_r} e^{-\chi_{r,s}/kT} \tag{3}$$

Where $n_{r,s}$ is the number of particles per cm^3, N_r is the total number density for particles in ionization stage r across all energy levels, $g_{r,s}$ is the statistical weight of the energy level, $\chi_{r,s}$ is the excitation energy measured from the ground level, k is the Boltzmann constant, T the temperature and U_r is the partition function and is defined as

$$U_r = \sum_s g_{r,s} e^{-\frac{\chi_{r,s}}{kT}} \tag{4}$$

Partition Function			
U_r	5000 K	10 000 K	20 000 K
U_1	1.1089	1.4559	2.2324
U_2	1.1089	1.4563	2.2714
U_3	1.1089	1.4563	2.2716
U_4	1.1089	1.4563	2.2716

Table 1: The partition function computed for different ionization stages and temperatures for the hypothetical element "Schadeenium"

The statistical weights and excitation energies used in table 1 are given by the hypothetical element "Schadeenium", named after Aert Schadee, who called it "E". It's statistical weights are $g_r = 1$ for all levels (r,s) and it's excitation energies increase incrementally by 1 eV. It has ionization energies $\chi_1 = 7$ eV for neutral E, $\chi_2 = 16$ eV for E^+, $\chi_3 = 31$ eV for E^{2+} and $\chi_4 = 51$ eV for E^{3+}.

For small temperatures, the exponent in equation 4 will be relatively large, and only the first few terms in the sum will contribute to the partition function. The higher order terms will be vanishingly small. However, for larger temperatures $\frac{1}{kT}$ will be smaller and the higher order terms won't vanish as quickly. This is why $U_1 = U_2 = U_3 = U_4$ for $T = 5000$K, but start diverging from each other for $T = 10000$K and are significantly different at $T = 20000$K, since the higher order terms come into play.

All the variables in the Boltzmann distribution are now known, and the population densities for the energy levels can be calculated.

Population densities of energy levels			
$n_{r,s}/N_r$	5000 K	10 000 K	20 000 K
$s = 1$	0.90	0.69	0.45-0.44
2	0.09	0.22	0.25
3	0.01	0.07	0.14
4	(-3)	0.02	0.08
5	(-4)	0.01	0.04
6	(-5)	(-3)	0.02
7	(-6)	(-3)	0.01
10	(-10)	(-5)	(-3)
15	(-15)	(-8)	(-4)

Table 2: Population densities of different energy levels and temperatures for Schadeenium.

As seen in table 2, the population decay is less steep for higher temperatures. This is because the exponent in equation 3 will be more negative for larger smaller values of T, and so $n_{r,s}/N_r$ will decay more quickly. The population decay for higher T will be less steep, as the exponent is less negative.

The Saha distribution gives the population density of various ionization stages of an element in TE.

$$\frac{N_{r+1}}{N_r} = \frac{1}{N_e} \frac{2U_{r+1}}{U_r} \left(\frac{2\pi m_e kT}{h^2} \right)^{3/2} e^{-\frac{\chi_r}{kT}} \tag{5}$$

Equation 5 gives the population density of the next ionization level. To calculate the population of all the ionization levels, the first stage N_1 is set to 1, and equation 5 is used to calculate the rest.

Population densities of the ionization stages				
N_r/N	ion	5000 K	10 000 K	20 000 K
$r = 1$	E	0.91	(-4)	(-10)
2	E^+	0.09	0.95	(-4)
3	E^{2+}	(-11)	0.05	0.63
4	E^{3+}	(-36)	(-11)	0.37
5	E^{4+}	(-82)	(-29)	(-6)

Table 3: Population densities for the different ionization stages. Here $N = \sum_r N_r$ is simply the sum of the population densities over all ionization stages.

Table 3 shows that for a given temperature, only two ionization stages are significantly present. This is because for low

temperatures (T = 5000 K), there will be quite a lot of neutral E. Since the temperature is low, the $e^{-\frac{\chi_r}{kT}}$ term in equation 5 will dominate, giving fewer and fewer atoms in each ionization stage as χ_r increases.

For higher temperatures (T=10 000 K, 20 000 K), there will be very few neutral atoms since the temperatures are high enough to ionize them. But since the temperature is so high, the next level will be more populated since the temperature term in equation 5 dominates. As χ_r increases, $e^{-\frac{\chi_r}{kT}}$ will start dominating, giving lower and lower population densities.

A comparison between table 2 and 3 might lead one to wonder why ionization can fully deplete a stage even though the Boltzmann distribution gives very low population densities at the higher energy levels. The answer lies in the electron pressure N_e. For a given temperature, the electron pressure can cause equality between the Boltzmann- and the Saha distribution.

2.3. Payne curves for Schadeenium

If Payne's assumption is correct, then one would expect spectral lines to have the same shape as the population density when plotted against temperature.

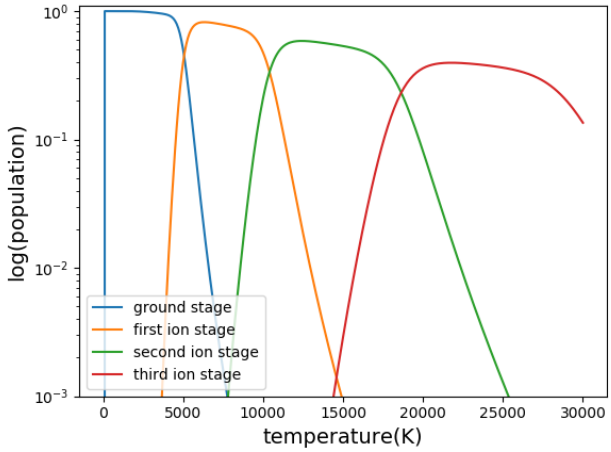

Fig. 3: $n_{r,1}/N$ plotted against temperature for different ionization stages r.

Figure 3 shows the relative population of the energy ground state, $n_{r,1}/N$. This is done by first finding the value of $n_{r,s}/N_r$ through the Boltzmann function and multiplying it with N_r/N, found using the Saha function. The location of the spectral line for a given ionization stage is determined by the Saha distribution. It is also responsible for the steepness in the wings of the populations. As temperature increases, the Boltzmann distribution will become more smoothed out and the population line will be flatter.

Figure 4 includes the population densities of $s = 2$ and $s = 3$ for the same ionization stages as in figure 3. The leftmost line of each color therefore represent the neutral state of E, while the rightmost lines represent the third ionization stage, E^{3+}.

The population of the ground state is about 10 times larger than that of the first excited state, which is about 10 times as populated as the second excited state.

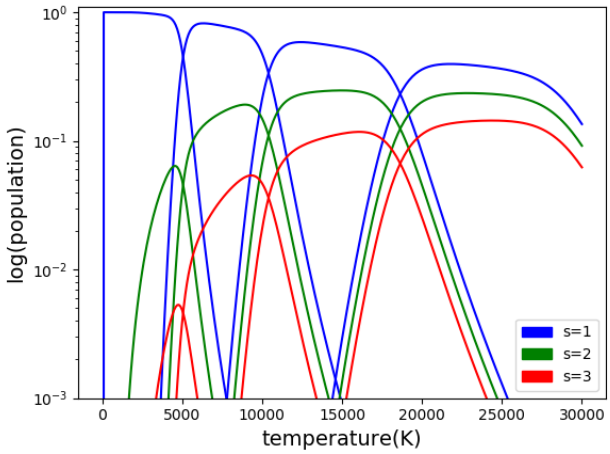

Fig. 4: $n_{r,s}/N$ plotted against temperature for the ionization stages E, E^+,E^{2+} and E^{3+}. The different energy level plots within each ionization stage are roughly aligned vertically.

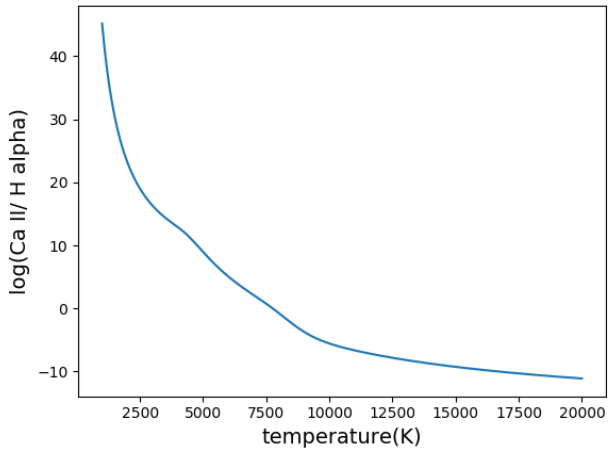

Fig. 5: Relative density of Ca^+ to H_α plotted against temperature.

2.4. Ca^+K vs H_α line strength

In figure 5, the population density of Ca^+ relative to H_α has been plotted against temperature. The reason why the solar Ca^+K line is so much stronger than the solar H_α line can be seen in this plot. The temperatures in the solar photosphere ranges between 4000 K and 6000K. For T = 5000 K, the population ratio was calculated to be 7663. This is because the Ca^+ line results from a transition from s=2 to the ground state, while the H_α line results from a transition from s=3 to s=2. Since the ground state of Ca^+ is more populated at these temperatures, the Ca^+ line will be stronger. This is shown more clearly in figure 6, where the relative population densities for the two elements has been plotted against temperature.

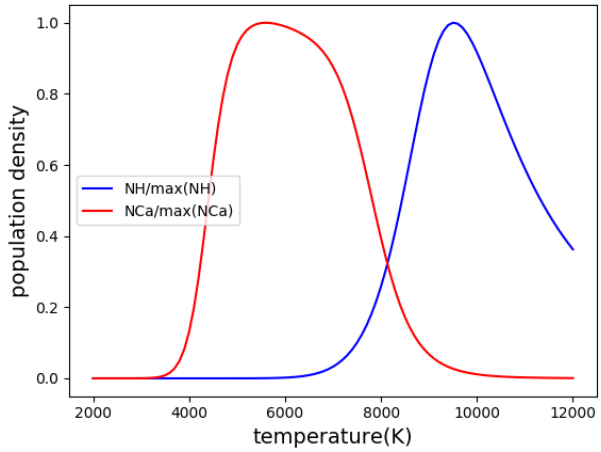

Fig. 6: Relative population density for Ca^+ and H_α plotted vs. temperature.

The temperature sensitivity is given by $\frac{\Delta n}{\Delta t}/n$. This is essentially the derivative of the population density divided by the population. As seen in the normalized plot for n, the maximum population density for Ca^+ is found at $T \approx 5600K$ and $T \approx 9500K$ for HI. This reflected in figure 7, but since the derivative of n with respect to T has been divided by n, the plot will be "flipped", giving minima at $T = 5600K$ and $T = 9500K$ instead of maxima. On either side of each dip, there is a $\Delta n > 0$ flank on the left and a $\Delta n < 0$ flank on the right. For stellar temperatures in the region of these flanks, the spectral lines will not be stable.

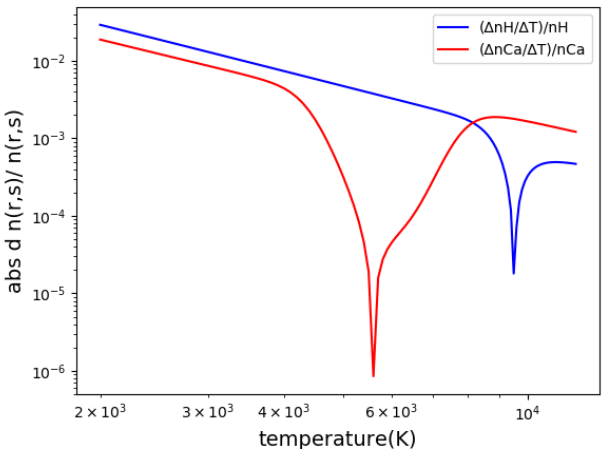

Fig. 7: Temperature sensitivity of the two elements plotted against temperature. This was done on a log-log scale to emphasize the dips.

Figure 8 shows the fraction of neutral hydrogen plotted against temperature for stellar atmospheres of electron pressure $P_e = 10^2$ dyne cm^{-2}. From the figure, the temperature for 50% ionization was found to be T = 9260 K.

.

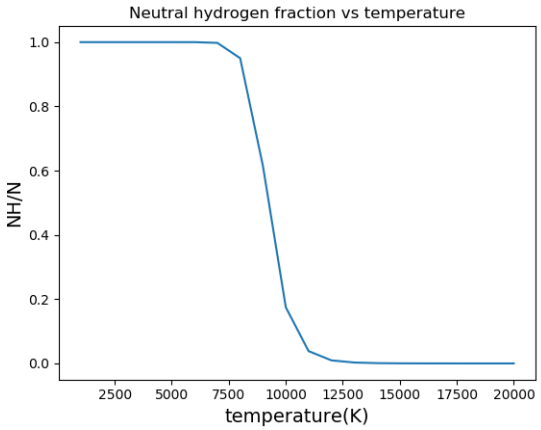

Fig. 8: Fraction of neutral hydrogen relative to the sum of population densities across all ionization stages plotted against temperature.

3. Discussion

The Boltzmann- and Saha distributions both assume thermodynamic equilibrium. While this holds in the stellar interior and reasonably well in the deeper parts of the stellar atmosphere, it does not hold in the chronosphere. This is due to the low density of the chronosphere, which allows radiation to easily escape.

The assumption that line strength scales linearly with population density is a false one. As will be seen, the line strength doesn't scale linearly, but through a curve of growth. The plots produced by Payne's assumption will therefore be similar, but not identical to observed spectral lines.

4. Conclusion

By making a few assumptions and applying the appropriate laws of physics, the morphological description of the Harvard sequence have been complemented by a physical model. This gives new insight into the formation of spectral lines. By the use of this physical model, the Hydrogen spectral lines in the Harvard sequence was determined to be the Balmer series, the relative strength of the Ca^+ line to that of the H_α line at T = 5000 K was found to be 7663 and the temperature for 50% ionization in stellar photospheres with electron pressure $P_e = 10^2$ dyne cm^{-2} was calculated to be 9260 K.

Fraunhofer Line Strength and the Curve of Growth

5. The Planck law

The Planck law is, along with the Wien displacement law and the Stefan-Boltzmann law, the radiation counterpart to the Boltzmann- and Saha distributions for matter. It states that the radiation intensity from a black body at a given wavelength and temperature is

$$B_\lambda(T) = \frac{2hc^2}{\lambda^5}\frac{1}{e^{hc/\lambda kT} - 1} \tag{6}$$

Where h is the Planck constant and k the Boltzmann constant. In figure 9, the Planck function is plotted against wavelength for a temperature of 8000 K.

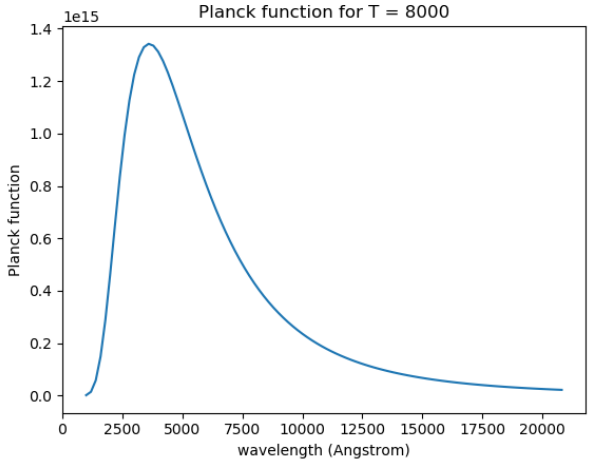

Fig. 9: The radiation intensity for a black body of temperature T = 8000 K plotted for against wavelength. The intensity increases steeply at low wavelengths, reaches a maximum at $\lambda_{max} \approx 3600$Å, then declines logarithmically towards zero.

Wien's displacement states

$$\lambda_{max} = \frac{b}{T} \tag{7}$$

Where b is a constant. Figure 10 shows how the Planck function behaves for different temperatures. Wien's displacement law is illustrated by the peaks shifting to the left for higher temperatures.

In figure 11 the logarithm of the intensity is plotted versus wavelength.

Figure 12 shows the planck function plotted against temperature on a log-log scale.

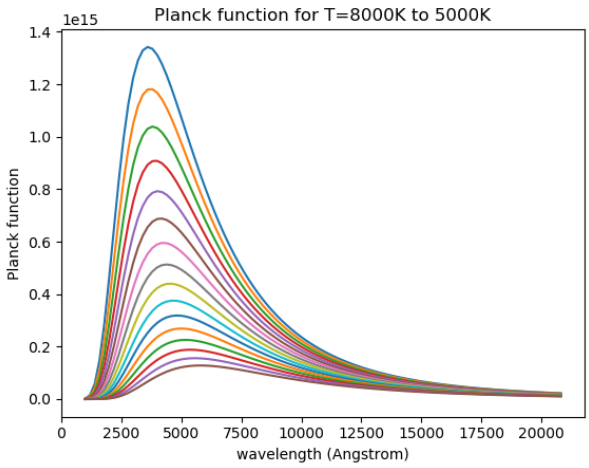

Fig. 10: The Planck function plotted for temperatures in the range 8000 K to 5000 K in increments of -200K. The uppermost blue line represents T = 8000 K while the lowermost brown line represents T = 5000 K. As seen, the total area under the curves increase for higher temperatures. This indicates that luminosity increases with temperature. The curve also gets more flattened for lower temperatures. This indicates that at lower temperatures, a black body will radiate more evenly across the wavelength spectrum then at higher temperatures, where the intensity will be stronger around λ_{max}. The figure also shows that λ_{max} gets shifted to lower wavelengths for higher temperatures. This is in accordance with Wien's displacement law, which states that the peak wavelength is inversely proportional to temperature.

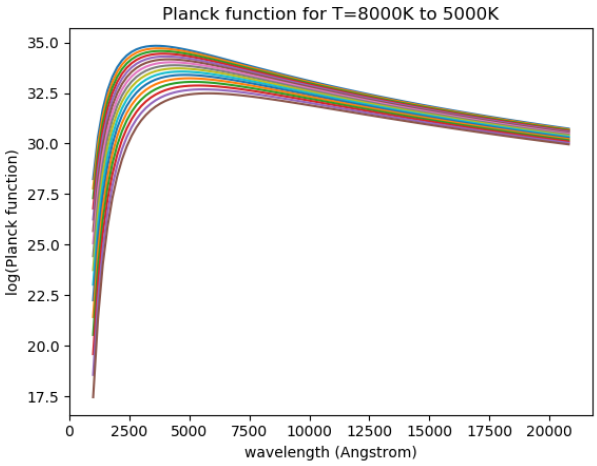

Fig. 11: $\log B_\lambda$ versus wavelength for the same temperatures as in figure 10. The steepness of the slope for small wavelengths and the slow decline for larger wavelengths is more protruding in this plot.

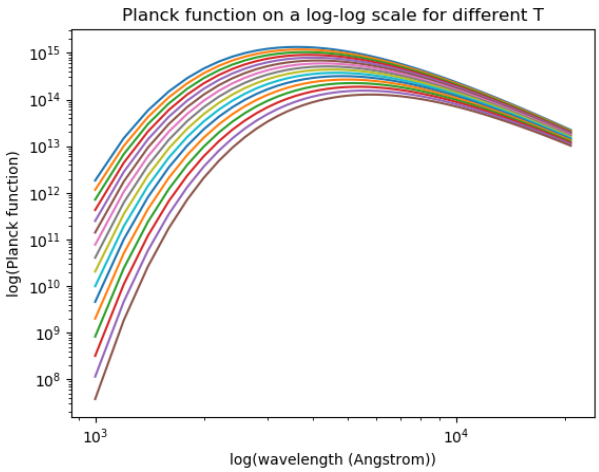

Fig. 12: The planck function plotted on a log-log scale. As seen, the intensities are quite different for smaller wavelengths, but converges at larger wavelengths.

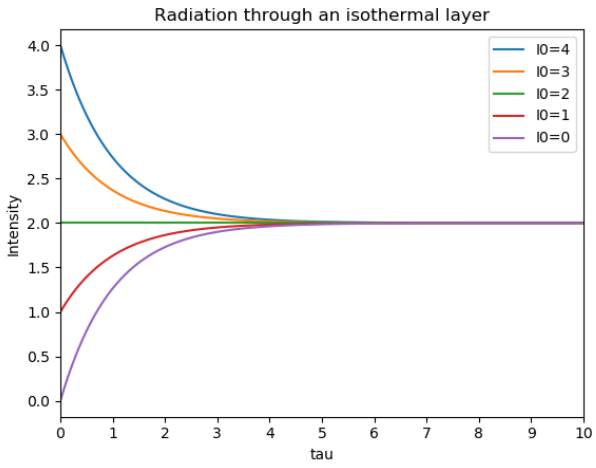

Fig. 13: Intensity versus optical thickness for different values of incoming intensity. B_λ was set to 2.

6. Radiation through an isothermal layer

When radiation passes through a layer of gas, the incoming intensity will be attenuated by a factor of $e^{-\tau}$ where τ is the optical thickness of the layer. Because the gas in the layer produces its own radiation with intensity B_λ, the term

$$B_\lambda[T(x)]\Delta\tau(x)e^{-(\tau-\tau(x))} \tag{8}$$

needs to be added when finding the emergent intensity. The $\Delta\tau$ term in equation 8 comes from the fact that a gas layer radiates better when it absorbs better. Integrating equation 8 over optical thickness and adding the attenuated incoming intensity yields the emergent intensity.

$$I_\lambda = I_\lambda(0)e^{-\tau} + \int_0^\tau B_\lambda[T(x)]e^{-(\tau-\tau(x))}d\tau(x) \tag{9}$$

For an isothermal layer, B_λ is independent of x, and it can be set outside the integral

$$I_\lambda = I_\lambda(0)e^{-\tau} + B_\lambda\left[e^{-(\tau-\tau(x))}\right]_0^\tau \tag{10}$$

Resulting in the expression for the emergent intensity for an isothermal gas layer of optical thickness τ

$$I_\lambda = I_\lambda(0)e^{-\tau} + B_\lambda\left(1-e^{-\tau}\right) \tag{11}$$

When $I_\lambda(0) = 0$ and $\tau << 1$, equation 11 can be taylor expanded to give $I_\lambda = B_\lambda(1-e^{-\tau}) \approx B_\lambda\tau$. Thus, $I_\lambda(\tau)$ will be approximately linear with τ. This is depicted in figure 13 by the purple line, but is more evident in figure 14.

For $\tau << 1$ the term $1-e^{-\tau}$ in equation 11 will be close to zero. The layer will therefore not radiate as a black body, as it lets most incoming light through. It is therefore called optically thin. For $\tau >> 1$, incoming radiation will not go through the layer. It is therefore called optically thick. As the intensity generated by each sub layer adds up, the emergent intensity will approach that of a black body. This is because as the number of sub layers increase, the total layer will become optically thick and the radiation generated in the "back" of the layer will be absorbed by all the sub layers in front of it. This is why the emergent intensities in figure 14 all approach B_λ at large τ.

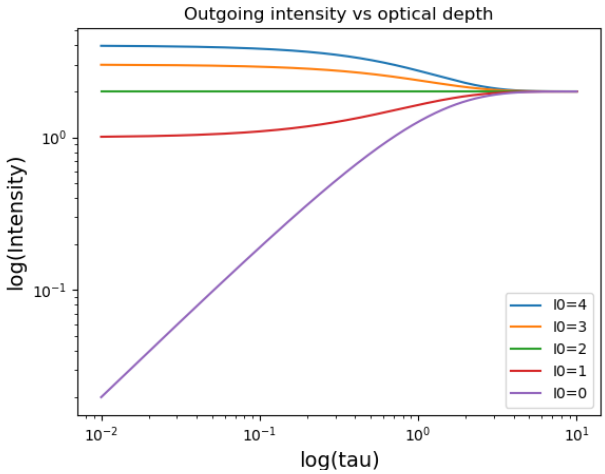

Fig. 14: Intensity versus optical thickness for different values of incoming intensity, plotted on a log-log scale. The linear scaling with τ for $I_0 = 0$ and $\tau << 1$ is very apparent.

7. Solar reversing layer

The optical thickness τ in equation 11 is in reality not an infinitely sharp delta function for a given wavelength, but is spread out in wavelength. This is in part due to Doppler shifts as the particles move away or towards the observer as well as Coulumb interactions with neighboring particles. Applying this gives a λ dependency for τ.

$$I_\lambda = B_\lambda(T_{surface})e^{-\tau_\lambda} + B_\lambda(T_{layer})\left(1 - e^{-\tau_\lambda}\right) \tag{12}$$

Where

$$\tau(u) = \tau(0)V(a,u) \tag{13}$$

Here $V(a,u)$ is the Voigt function. It is given by

$$V(a,u) \equiv \frac{1}{\Delta\lambda_D\sqrt{\pi}}\frac{a}{\pi}\int_{-\infty}^{\infty}\frac{e^{-y^2}}{(u-y)^2+a^2}dy \tag{14}$$

And is a convolution between a Gaussian and a Lorentzian distribution. Here $\Delta\lambda_D$ is the doppler width, u measures the wavelength separation from the line center in dimensionless units while the parameter a measures the amount of Coulomb disturbances. It has a damping effect. This effect increases with a, which can be seen in figure 15.

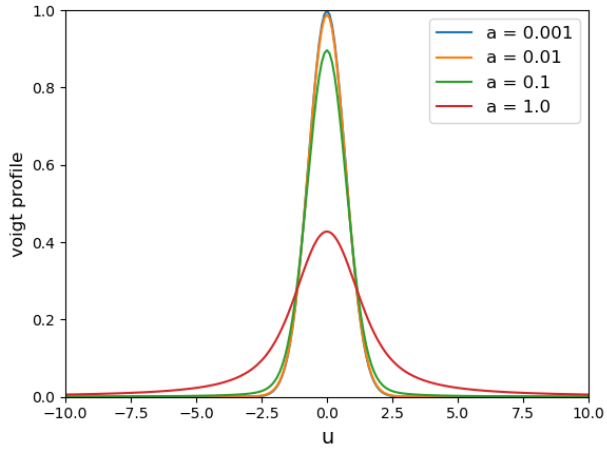

Fig. 15: The Voigt profile plotted against wavelength separation for different values of the damping parameter. The Voigt function is a convolution of a Gaussian- and a Lorentzian distribution. The peaks shown are caused by the Gaussian function, while the damping effect is a result of the Lorentzian function.

Figure 16 illustrates this damping effect more clearly.

In figure 17, the emerging intensity through the layer for a wavelength of $\lambda = 5000$Å is shown.

For $\tau(0) << 1$, the optical thickness of the inversion layer will be very small and let most radiation through. One therefore gets a dip in the intensity at the wavelength of absorption, but most of radiation passes through. This is seen in figure 18.

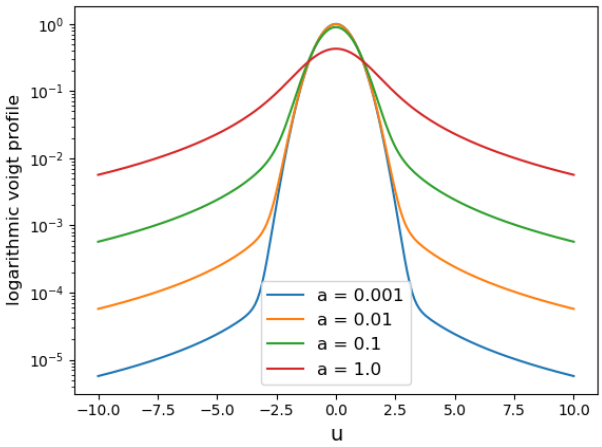

Fig. 16: The Voigt profile plotted on a log-log scale. The damping caused by a is more apparent in than in figure 15. The wings of the Voigt function grows with increasing a.

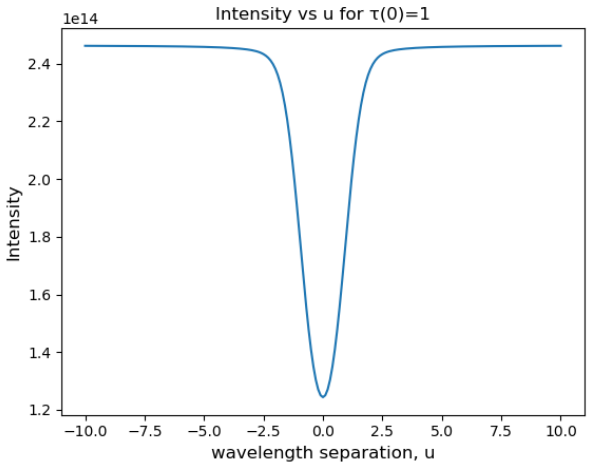

Fig. 17: Emergent intensity versus wavelength separation. Instead of a delta function at $u = 0$, one gets a dip around $u = 0$ due to the Voigt profile.

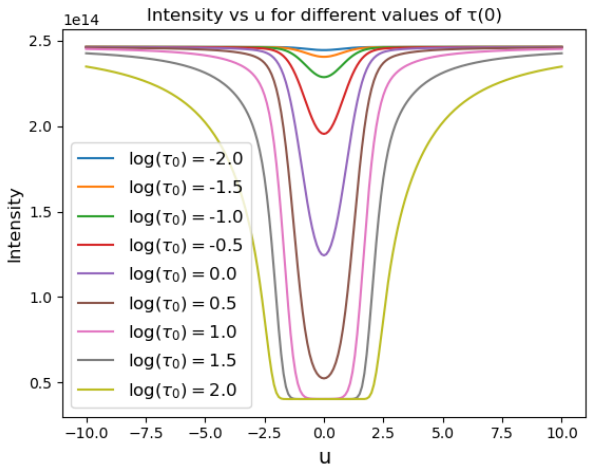

Fig. 18: Intensity versus wavelength separation for different values of $\tau(0)$. The plot shows a low intensity saturation limit for $\tau_0 >> 1$. This is due to the fact that the inversion layer also generates radiation. As τ_0 increases, this is the only radiation that comes through the inversion layer at the absorption wavelength. As the saturation limit is reached, increasing the optical pathlength $\tau(0)$ will no longer decrease the outgoing intensity at absorption wavelength. It will however broaden the line wings, since the incoming radiation has to pass through more gas, and will therefore encounter more high-velocity particles that contribute to reduce the outgoing intensity around the absorbtion wavelength.

8. Equivalent width and the curve of growth

The equivalent width was first introduced by Marcel Minnaert and his co-workers. It is a line-strength parameter that measure the growth of the dips seen in figure 18, called the curve of growth. It is given by

$$W_\lambda = \int \frac{I_{cont} - I(\lambda)}{I_{cont}} d\lambda \tag{15}$$

and is equal to the width of a rectangular piece of spectrum that blocks the same amount of spectrum completely. In figure 19 the absorption line for wavelength $\lambda = 5000$Å has been plotted. The integrand of equation 14 is called the relative width, and is simply a measure of how deep the spectral line is. The relative depth of the spectral line in figure 19 is plotted in figure 20.

Figure 21 shows the curve of growth for a wavelength of $\lambda = 5000$Å. It is a measure of how large the dip in the intensity is for different values of τ_0.

References

[1] R.J. Rutten. Stellar Spectra A, Basic Line Formation. August 7, 2010

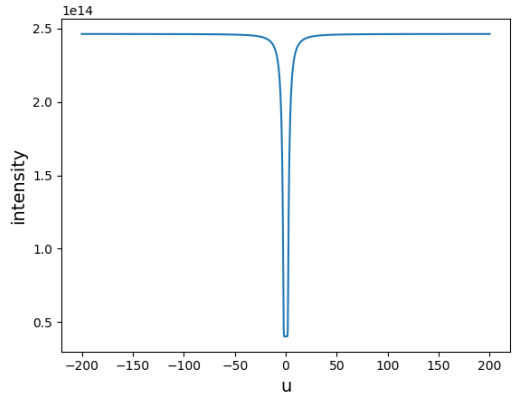

Fig. 19: Emergent intensity versus wavelength separation for $a = 0.1$. The plot shows that the sum of the incoming intensity and the intensity of the generated layer is $I_{cont} \approx 2.5e14$, whilst the intensity of the generated layer is $B_\lambda(T_{layer}) \approx 5e13$

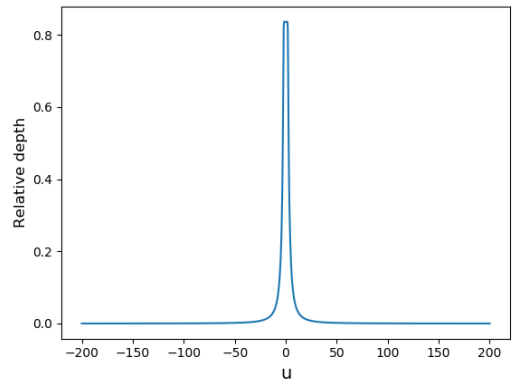

Fig. 20: Relative depth versus wavelength separation. As expected, this plot is the scaled inverse of figure 19.

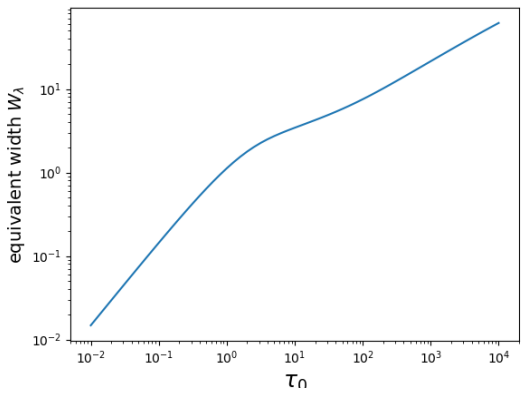

Fig. 21: Equivalent plotted against τ_0. The plot can divided into three parts. In the first part, the equivalent width is growing quite fast, as it has not yet reached the saturation limit. In the second part, the equivalent width has reached the saturation limit, but τ_0 is not yet large enough to develop wings in the intensity plot, so the slope is quite flat. In the third part, τ_0 is very large and the wings are developed. This causes a steeper slope, but not as steep as for small τ_0.